Assessment of grid anisotropy effects on LES models with different length scales

Jan-Erik Schumann*
German Aerospace Center (DLR), 37073 Goettingen, Germany

Siavash Toosi† and Johan Larsson‡
University of Maryland, College Park, MD 20742, USA

The effect of the eddy viscosity length scale on the accuracy of large eddy simulation (LES) is investigated for several commonly used subgrid models. Multiple types of length scales are considered, both purely geometric length scales (including the cube-root of the cell volume and the maximum cell dimension) and length scales that depend on both the grid and the flow. The assessment is focused on how the LES prediction changes for increasingly anisotropic grids, in forced isotropic turbulence and channel flow at high Reynolds number. While some length scales perform better than others, the main conclusion is that no single length scale produces LES results that are completely independent of the grid anisotropy. Since every model and length scale tested produces accurate results on at least one grid and inaccurate results on at least one other grid, the study shows clearly the need to assess LES models on multiple grids with multiple different anisotropy ratios.

I. Nomenclature

C	=	Model constant
c_f	=	Friction coefficient
dev	=	Deviatoric part
D, DSM	=	Dynamic Smagorinsky Model
DNS	=	Direct Numerical Simulation
g_{ij}	=	Velocity gradient
h_{wm}	=	Wall model height
i, j	=	indices indicating coordinate direction
k	=	Wave number
N	=	Number of grid points

*PhD Researcher, Spacecraft Department, Institute of Aerodynamics and Flow Technology.
†Postdoctoral Associate, Department of Mechanical Engineering. AIAA Member.
‡Associate Professor, Department of Mechanical Engineering, AIAA Senior Member.

num	=	numerical
S_{ij}	=	Strain rate
u_i	=	Velocity component
U	=	Streamwise mean velocity
V, Vr	=	Vreman model
VD	=	Van-Driest transformation
W, WALE	=	Wall-Adaptive Local Eddy-Viscosity model
x, y, z	=	Coordinate directions
α	=	Design of experiment coefficient
δ	=	Channel half-width
δ_{ij}	=	Kronecker delta
Δ	=	Filter width / Length scale
$\widehat{\Delta}$	=	Test filter width
$\Delta x, \Delta y, \Delta z$	=	Grid spacings
γ	=	Filter ratio
κ	=	von Karman coefficient
κ_{scaled}	=	Scaled von Karman coefficient
μ_{sgs}	=	Eddy viscosity
R_{ij}	=	Reynolds stress
τ_w	=	Wall shear stress

II. Introduction

The increase in computing power has expanded the envelope of problems that can be computed using large eddy simulation (LES), and has paved the way to take advantage of the presumably higher accuracy in complex flows and geometries. This move towards ever more complex geometries often leads to the use of increasingly anisotropic grids, which raises the question of how to define the length scale that is required in any eddy viscosity model. This length scale theoretically corresponds to the cut-off between resolved and unresolved scales, but the cut-off length scale is not easily defined on anisotropic grids. In practice, the coarse-graining is often achieved implicitly through the discretization on the grid, and thus the effective implied filter is essentially unknown. While some methods/codes use an explicit filter, e.g., to control aliasing errors, these filters retain the same or similar anisotropy as the underlying grid.

Many types of subgrid models are theoretically capable of correctly modeling the subgrid stress on anisotropic grids, including tensorial eddy viscosity models [1, 2], approximate deconvolution models [3], and models based on

Taylor expansions [4, 5]. The most common subgrid modeling approach in practice, however, is to use a scalar eddy viscosity, which is defined as the product of a length scale Δ and a velocity scale. This then requires the definition of a scalar length scale Δ from an underlying anisotropic grid (or, more generally, filter-width field).

Very little research is available as to how these definitions affect the turbulence on a fundamental level [2]. Most proposed new length scales are directly applied to more complex flows and only their overall impact on the results is evaluated [6, 7]. Trias et al. [8] introduced a new length scale and in the process investigated several length scale definitions for comparison, testing decaying isotropic turbulence, wall-resolved channel flow and the flow around a square cylinder. In the current paper their findings are extended in several different ways. First, the present study uses different eddy viscosity models as well as an additional length scale which are introduced and compared *a priori* in Section III. Secondly, the investigation includes a comparison between the dynamic Smagorinsky model and constant coefficient models. Finally, the current investigation uses high Reynolds number test cases, specifically forced isotropic turbulence (Section IV) and wall-modeled channel flow (Section V), and aims for a more fundamental understanding of the processes that determine the behavior of LES on anisotropic grids. The primary focus in these investigations is to study the robustness of the investigated filter length definitions, i.e., their sensitivity to anisotropic grids. The absolute accuracy on a particular grid, on the other hand, is also dependent on the underlying subgrid scale model and can be improved by tuning of the model for that particular grid.

III. Methodology

A. Subgrid scale models

The present work only considers the class of scalar eddy viscosity models where the deviatoric part of the subgrid scale stress tensor τ_{ij} is modeled as

$$\tau_{ij}^{\text{dev}} = \tau_{ij} - \frac{1}{3}\tau_{kk}\delta_{ij} = -2\mu_{\text{sgs}}S_{ij}^{\text{dev}},$$

where μ_{sgs} is the scalar eddy viscosity, $S_{ij} = (g_{ij} + g_{ji})/2$ is the resolved rate-of-strain tensor, and $g_{ij} = \partial u_i/\partial x_j$ is the resolved velocity gradient tensor. The deviatoric part of S_{ij} is $S_{ij}^{\text{dev}} = S_{ij} - (S_{kk}/3)\delta_{ij}$. In the present work we consider three different popular models: the Vreman model [9], the Wall-Adapting Local Eddy-Viscosity (WALE) model [10], and the dynamic Smagorinsky model [DSM; 11].

The dynamic Smagorinsky model [11, 12] computes the eddy viscosity as

$$\mu_{\text{sgs}}^{\text{DSM}} = \rho C_{\text{D}}\Delta^2 |S|,$$

where $C_{\text{D}}\Delta^2$ is computed from the Germano identity after a test-filtering operation. Models that use the dynamic procedure are frequently referred to as having no user-specified constants, but this is not quite true: the process does

require the specification of the test-filter, specifically whether the test-filter is isotropic or not (e.g., test-filtering in wall-parallel planes is considered the norm in channel flows) and also the ratio of the test-filter width $\widehat{\Delta}$ to the underlying implied filter width Δ. This ratio (say $\gamma = \widehat{\Delta}/\Delta$) is never unambiguously defined in practice, and should thus be viewed as a user-defined parameter. In addition, dynamic procedures often require clipping to avoid negative eddy viscosity. The other subtle point is that the dynamic procedure computes the combined product $C_{\mathrm{D}}\Delta^2$, which implies that a specific length scale definition is not needed if the test-filter is an isotropic coarsening operation, i.e., if the test-filter increases the cut-off length scale of the solution in every direction by an equal factor. This is rarely true in practice, either due to test-filtering only in certain directions or (most commonly) due to imperfect knowledge of what the cut-off length scale of the actual LES method is in each direction. When the test-filter does not correspond to isotropic coarsening, a length scale definition is needed in order to compute the appropriate filter-width ratio γ. The effects of this subtle fact are explored in sections IV.C.2 and V.D.

The eddy viscosity model proposed by Vreman [9] is defined as

$$\mu_{\mathrm{sgs}}^{\mathrm{Vr}} = \rho C_{\mathrm{V}} \sqrt{\frac{B_\beta}{g_{ji}g_{ji}}} \quad , \quad \beta_{ij} = \Delta_m^2 g_{im} g_{jm} \ , \quad B_\beta = \beta_{11}\beta_{22} - \beta_{12}^2 + \beta_{11}\beta_{33} - \beta_{13}^2 + \beta_{22}\beta_{33} - \beta_{23}^2 ,$$

where the coefficient C_{V} is a model parameter. This model incorporates a length scale definition directly into the model by incorporating the grid spacing into B_β. This makes the Vreman model theoretically suitable to use in anisotropic turbulence (statistically different g_{ij} for different i and j) and on anisotropic grids (different Δ_m in different directions).

The Wall-Adapting Local Eddy-Viscosity (WALE) model [10] computes the eddy viscosity as

$$\mu_{\mathrm{sgs}}^{\mathrm{WALE}} = \rho \left(C_{\mathrm{W}}\Delta\right)^2 \frac{\left(\mathcal{S}_{ij}^d \mathcal{S}_{ij}^d\right)^{3/2}}{\left(S_{ij}S_{ij}\right)^{5/2} + \left(\mathcal{S}_{ij}^d \mathcal{S}_{ij}^d\right)^{5/4}} \quad , \quad \mathcal{S}_{ij}^d = \frac{1}{2}\left(g_{ij}^2 + g_{ij}^2\right) - \frac{1}{3}\delta_{ij} g_{kk}^2 ,$$

where the constant C_{W} is a model parameter, δ_{ij} is the Kronecker delta, $g_{ij}^2 = g_{ik}g_{kj}$, and the length scale Δ has to be specified explicitly.

B. Length scale definitions

Different length scale definitions have been proposed in the literature over the years. One distinction between length scales is whether they depend purely on the geometry of the grid or whether they also depend on the flow. Important examples of the former type are the cube-root of the cell volume [13]

$$\Delta_{\mathrm{vol}} = \sqrt{\Delta_x \Delta_y \Delta_z} ,$$

the maximum size of the cell [14]

$$\Delta_{\max} = \max\left(\Delta_x, \Delta_y, \Delta_z\right),$$

and the L^2 norm of the cell size

$$\Delta_{\mathrm{L2}} = \frac{1}{\sqrt{3}}\sqrt{\Delta_x^2 + \Delta_y^2 + \Delta_z^2},$$

where Δ_x, Δ_y and Δ_z are the cell dimensions in different directions of a hexahedral cell (we use the special case of a Cartesian grid here).

For an isotropic cell, all these length scale definitions compute the same length scale corresponding to the cell size in the different directions. However, if one or two directions are repeatedly refined the definitions start to differ, e.g., with $\Delta_{\mathrm{vol}} \to 0$ and $\Delta_{\max} \to \Delta_x$ for $\Delta_y, \Delta_z \to 0$. Intuitively, neither of these behaviors seem correct in general. For example, for the case of isotropic turbulence and an initially isotropic grid, refining in two directions could possibly decrease the effective length scale at first but would eventually stop doing so. The length scale should, therefore, approach a value possibly smaller than the maximum grid spacing but certainly larger than zero. However, in the early stages of a shear flow where two-dimensional structures are predominant, only the resolution in the plane resolving these structures should be relevant. A possibly larger grid spacing in the direction of the vorticity vector should not impact the resolved turbulence and thus, for continued refinement in the two other directions, the effective length scale should continue to decrease.

In an effort to improve on the purely geometric definitions, several flow-dependent definitions have been developed, of which the most popular are briefly introduced in the following. For further details on each definition the reader is referred to the respective publication. The first definition is based on the vorticity vector ω_i as [6]

$$\Delta_\omega = \frac{1}{|\omega|}\sqrt{\omega_x^2\Delta_y\Delta_z + \omega_y^2\Delta_x\Delta_z + \omega_z^2\Delta_x\Delta_y},$$

which essentially computes the square-root of the area of the cell in the direction normal to the vorticity vector. An improved version was proposed by Mockett et al. [7] as

$$\widetilde{\Delta}_\omega = \frac{1}{\sqrt{3}}\max|l_n - l_m|,$$

where $l_n = \omega/|\omega| \times r_n$ and r_n are vectors from the cell centroid to every corner of the cell. More recently, Trias et al. [8] proposed

$$\Delta_{\mathrm{lsq}} = \sqrt{\frac{\beta_{ij}\gamma_{ij}}{\gamma_{ij}\gamma_{ij}}},$$

where $\gamma_{ij} = g_{ik}g_{jk}$. This length scale is based on the Clark model [4] and has similarities with the Vreman model [9].

C. *A priori* assessment of the length scales

The behavior of the different length scale definitions can be qualitatively compared *a priori* by analyzing them for different aspect ratios of "pancake" and "pencil" cells: the former are the result of refinement in a single direction while the latter are the result of refinement in two directions. The flow-dependent length scales are computed based on a field of isotropic turbulence.

The computed length scales differ significantly between the definitions. $\Delta_{\max}$ computes the largest length scale whereas Δ_{vol} quickly approaches very small values; at an aspect ratio of one hundred, Δ_{vol} is about 5 and 25 times smaller than $\Delta_{\max}$ for pancake and pencil cells, respectively. Assuming the same flow field and thus strain rate tensor, this would lead to an eddy viscosity that is 25 and 625 times smaller. Note that these types of high aspect ratio cells are not uncommon in applied flows, e.g. near the nozzle lip in a jet. Δ_{L2} converges to a constant value 15% and 40% smaller than $\Delta_{\max}$ for pancake and pencil cells, respectively. As pointed out by Trias et al. [8] $\widetilde{\Delta}_\omega$ and Δ_{lsq} behave similarly for these flow conditions, showing a fast convergence to a constant value of $\Delta/\Delta_{\max} \approx 0.8$ at aspect ratios around 10 and $\Delta/\Delta_{\max} \approx 0.5$ at aspect ratios around 30 for pancake and pencil cells, respectively. For pancake cells, the Δ_ω definition behaves qualitatively similarly as well, but for pencils cells the behavior is more akin to Δ_{vol} (if slightly less extreme), which was one of the reasons for the development of $\widetilde{\Delta}_\omega$ [7].

The length scales Δ_{vol}, $\Delta_{\max}$, $\widetilde{\Delta}_\omega$ and Δ_{lsq} are chosen for further investigation. Δ_{vol} and $\Delta_{\max}$ yield the two most extreme cases (smallest and largest length scales, respectively) and thus can serve as a lower and upper limit. $\widetilde{\Delta}_\omega$ and Δ_{lsq} show behaviors that most correspond to intuition and also showed the most promising results when investigated by Trias et al. [8]. Thus it is of interest to further study their detailed behavior as well as possible still existing shortcomings.

D. Numerical method

The main code used in this study is the *Hybrid* code which solves the compressible Navier-Stokes equations for a calorically perfect gas on structured Cartesian grids. A sixth-order accurate central difference scheme is used for the convective terms, applied in the split form by Ducros et al. [15] (skew-symmetric in the limit of zero Mach number) for reduced aliasing errors and improved numerical robustness. The diffusion terms are discretized in a finite-volume-like manner that is conservative yet produces maximum modified wavenumber for the most poorly resolved modes. The viscosity is assumed to follow the power-law $\mu = \mu_{\text{ref}} (T/T_{\text{ref}})^{3/4}$, and the Prandtl number is taken as $Pr = 0.7$. Numerical noise is removed by a numerical sixth-order hyper-viscosity term in conservative form [16]. Time-integration is handled by classic fourth-order Runge-Kutta. For the simulations with the dynamic procedure, the test-filtering is performed using a seven-point filter by Vasilyev et al. [17]. The code has been used in multiple prior studies, including of channel flows [cf. 18].

IV. Forced isotropic turbulence

The appeal of isotropic turbulence as a test case for assessing grid anisotropy is that the optimal grid is known (a uniform isotropic grid) and that any deviation from the results on this optimal grid reveals an imperfection in the subgrid modeling. The main reason for using forced (rather than decaying) isotropic turbulence is that it allows the turbulence to reach a fully developed state. In contrast, decaying turbulence retains a memory effect from the initial (often randomized and thus not truly physical) turbulence, and thus any errors at any time $t > 0$ may be related more to the initial condition and the initial development than anything else. For example, if the randomized initial "turbulence" initially decays faster than realistic turbulence, the "best" subgrid model would be one that slightly underpredicts the decay.

A. Problem set-up

The isotropic turbulence is created in a periodic domain of size $(2\pi)^3$ by a forcing field confined to the smallest wave numbers with slowly drifting random phase angles. The resulting turbulence can be tuned by the target dissipation rate, the fluid properties, and the wave numbers at which the fluctuations are introduced. In the present study, these parameters are tuned to achieve a Reynolds number of $\mathrm{Re}_\lambda = 2400$ and a turbulent Mach number of $M_t = 0.08$. A corresponding direct numerical simulation (DNS) grid would require more than 4000^3 points.

At steady state, the turbulence spectrum is the only meaningful quantity to analyze. No additional insight was found when considering one- or two-dimensional spectra, and thus only the three-dimensional energy spectra are shown here. The smallest wave numbers are significantly affected by the forcing and thus cannot be used for evaluation; for the applied settings, an effect of the forcing in the energy spectrum for wave numbers $k \lesssim 6$ was observed. After an initial transient, the remainder of the spectrum achieves a quasi-steady state that then allows for averaging over several snapshots.

The investigated grids are defined by the number of points in the x, y, and z directions, as N_x, N_y, and N_z, respectively. An isotropic grid with $N_x = N_y = N_z = 64$ is chosen as the base grid. This base grid is refined to create pancake cells by increasing N_z up to 1024 and pencil cells by increasing N_y and N_z simultaneously up to 512. Thus aspect ratios of up to 16 for pancake cells and up to 8 for pencil cells are achieved.

The coefficients in the constant coefficient models are tuned so that the solutions on the base grid agree well with the reference solution. This tuning resulted in model coefficients of $C_\mathrm{V} = 0.052$ and $C_\mathrm{W} = 0.40$. Minor deviations due to inherent model differences as well as limiting of the model constant tuning to two significant digits remain, but should not affect the analysis.

B. Definition of correct results: the "isotropic region"

Previous studies show that the dynamic Smagorinsky model yields accurate results for isotropic turbulence on isotropic grids. Thus, instead of computing an expensive DNS, a series of computations on isotropic grids with 64^3,

128^3, 256^3 and 512^3 points are used as the reference. The reference spectra collapse on each other for at least the lowest 1/4 of the resolved wave numbers, and arguably up to the lowest 1/2 of them. Since three-dimensional spectra can only be computed for $k < \min\left\{N_x/2, N_y/2, N_z/2\right\}$, the spectra on the anisotropic grids are limited to $k < 32$, and these spectra are evaluated for $6 < k < 32$. In this wave number range, the finest DSM results on isotropic grids yield sufficient accuracy to act as the reference solution.

An optimal model should approach the finest reference solution with each refinement, independent of whether one, two or three directions are refined. However, to expect the results on anisotropic grids to immediately agree with the correct solution would be an unfair expectation, considering that even the isotropic refinement - obviously the optimum for the case of isotropic turbulence - does not immediately yield exact agreement between different refinement levels at the highest wave numbers. Additionally, even how much the spectrum on each anisotropic grid should differ from either the base grid or an isotropically refined grid is unknown. Therefore, it seems sensible to only require two properties from a good length scale definition on an anisotropically refined grid: (i) it should not produce worse agreement with the reference solution than the base grid; and (ii) it should not have a larger effect than any level of isotropic refinement might have. Hence, anisotropic refinement should yield a spectrum that lies between those of the isotropically refined grids and that of the base grid; e.g. the spectra on $64\times64\times256$ and $64\times256\times256$ grids should lie somewhere between the spectra obtained for 256^3 and 64^3 grids.

This allows us to define a region, in the following called the "isotropic region", that is limited by the reference spectra on finer isotropic grids and the spectra on the base grid using the same subgrid model. Any result in this "isotropic region" should be considered a valid model response to anisotropic refinement of the grid. This region is also displayed as a grey region in the spectra shown in the following.

The definition of this region also allows for a better quantitative evaluation of different models. Since a model's spectrum would optimally remain in the isotropic region under anisotropic refinement, it is possible to compute the absolute deviation from this region at each wave number and use the sum of the absolute deviations as a quantitative measure for the behavior of the model. This error metric can then be plotted over the aspect ratio for pancake and pencil cells, respectively, as is shown later in Fig. 4. The advantage of metric over e.g. the total turbulent kinetic energy is that it is possible for a model to show the correct amount of turbulent kinetic energy, but still differ from the correct spectrum by underpredicting the turbulent kinetic energy in one wave number range and overpredicting it in another.

C. Dynamic Smagorinsky model

The investigation of the dynamic Smagorinsky model is split into two parts, with the first investigating the behavior when 3D test filtering is used and the second investigating the case of test filtering in less than 3 directions.

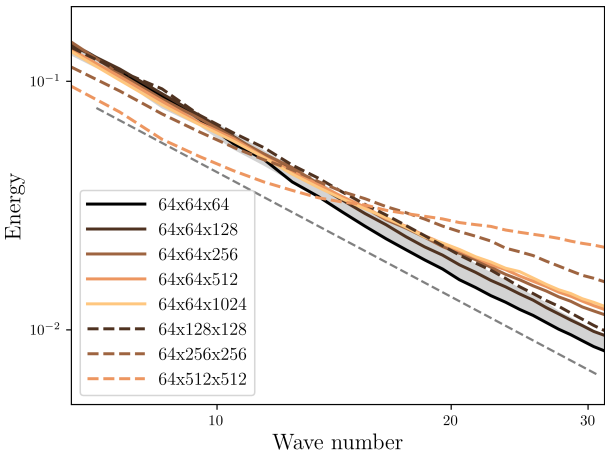

Fig. 1 Spectra for the dynamic Smagorinsky model with 3D filtering on anisotropic grids. Solid lines show grids with pancake cells, dashed lines show grids with pencil cells.

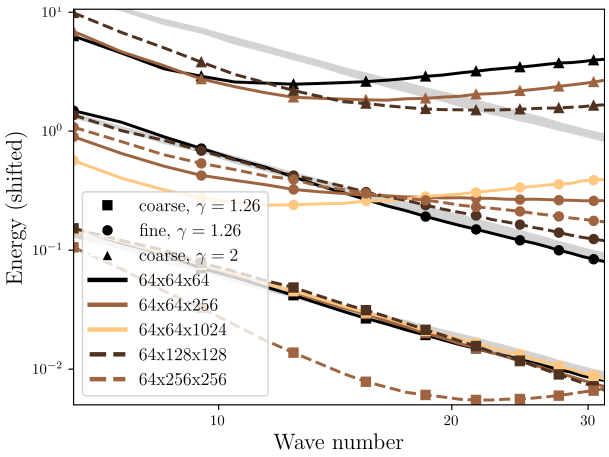

Fig. 2 Comparison of spectra for the dynamic Smagorinsky model with 1D filtering, vertically shifted for improved clarity. The labels *coarse* and *fine* denote which direction the 1D filtering was applied to.

1. Test filtering in three directions

The resulting spectra on different anisotropic grids using the dynamic Smagorinsky model with 3D filtering are shown in Fig. 1. Additionally, the isotropic region that was described in the previous subsection is indicated as a grey region. An energy pile up at high wave numbers with increasing anisotropy is clearly visible, with pencil shaped cells showing a more extreme behavior than pancake shaped cells. This behavior is created by a too strong reduction of eddy viscosity that does not correspond to the increase of resolved turbulent features.

For pancake shaped cells the spectra seem to converge and little further changes are expected for larger aspect ratios than the ones investigated. However, for the pencil shaped cells the energy pile up is so large that it also affects smaller wave numbers and no clear convergence limit is visible yet.

This shows that even though the dynamic procedure can adapt the coefficient it is still significantly affected by grid anisotropy.

2. Test filtering in less than three directions

Another consideration is the behavior of the dynamic Smagorinsky model for other than 3D filtering. This might become necessary if the flow field is not globally isotropic and thus filtering has to be restricted to 1 or 2 directions. In the following the behavior for 1D filtering is investigated since it allows a clear distinction between the refined and non-refined directions. A qualitatively similar behavior was observed in preliminary studies using 2D filtering and thus is not shown here. A reduced number of grids is investigated for 1D filtering since the behavior becomes quickly visible. The spectra are displayed in Fig. 2.

An important factor when considering non-isotropic filtering is the effect of the filter ratio γ. As described in

Sec. III.A, the dynamic Smagorinsky model is often referred to as having no user-specified constant, but in reality γ has to be specified. For 3D filtering $\gamma = 2$ leads to correct results, but for 1D filtering a significant energy pile up and an unphysical energy spectrum are obtained with this value as shown in Fig. 2 (top set of curves). For this case even on the base grid a significant energy pile up is visible, indicating that the error is not due to anisotropy. Interestingly, the energy pile up decreases with increased anisotropy, the opposite behavior observed for the 3D filtering.

To obtain the correct spectra on the base grid for 1D, the filter ratio for 1D filtering has to be adjusted to $\gamma = 2^{1/3} \approx 1.26$. This indicates that the filter-ratio has to be adapted if the number of filtering directions is changed.

The bottom set of spectra in Figure 2 shows the result if test filtering is only applied in the x direction, i.e., the direction that is never refined. On the base grid the spectra agrees with the reference, but upon anisotropic refinement the turbulent kinetic energy at high wave numbers is slightly reduced, indicating a slightly too large eddy viscosity. This is due to the limitation of the test filtering to the coarsest direction which neglects possibly better resolved turbulence in the fine directions. However, with further refinement the solution improves again, indicating that for very high aspect ratio pancake cells only considering the coarsest direction might be sufficient. The results for pencil cells with aspect ratio 2 shows very similar results to the pancake cells. However, for pencil cells with aspect ratio greater than two the eddy viscosity for this model variant drops to zero and a strong change in spectral behavior appears as a consequence. This behavior is repeatable on different grids - starting at aspect ratios of about three - and for different settings, including a restart from a correct solution. No definitive explanation or the exact reason for this behavior could be found by the authors.

The middle set of spectra in Figure 2 displays the result if test filtering is only applied in the z direction, i.e., the always (for both pancake and pencil cells) refined direction. Energy pile up at high wave numbers is clearly visible again, with the spectra for pencil cells comparable to, but marginally worse than, those obtained for 3D filtering. However, the pancake cells show a significantly worse behavior; so much that these spectra deviate further from the isotropic region than those obtained on grids with pencil cells. This changed behavior between 1D and 3D filtering for pancake cells can be explained by the fact that the two coarse directions are included in the 3D filtering whereas the 1D filtering exclusively considers the fine direction. Therefore, the eddy viscosity is reduced much more for 1D filtering, leading to a more extreme energy pile-up. For the pencil cells the difference between 1D and 3D filtering is less pronounced since two fine and one coarse direction (3D) compared to one fine direction (1D) are considered.

D. Constant coefficient models

All investigated constant coefficient models and length scale definitions, with the exception of $\Delta_{\max}$ (for which the opposite is the case), compute a too low eddy viscosity upon anisotropic grid refinement and thus show an energy pile up qualitatively similar to that for the dynamic Smagorinsky model with 3D filtering. However, how large this pile up is differs from length scale to length scale. This is qualitatively visible when comparing the spectra computed with $\widetilde{\Delta}_\omega$,

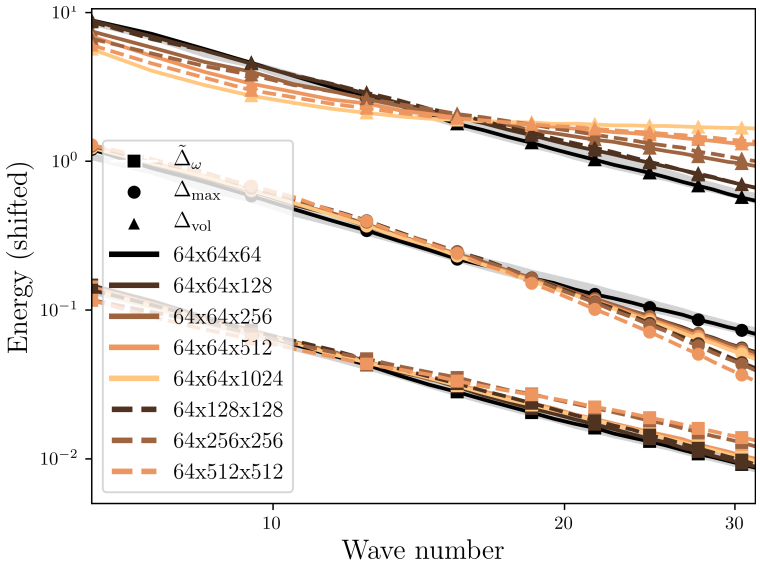

Fig. 3 Comparison of spectra for WALE with the $\widetilde{\Delta}_\omega$ (lower curves), $\Delta_{\max}$ (middle) and Δ_{vol} (upper) length scales.

$\Delta_{\max}$ and Δ_{vol} in Fig. 3.

To allow for a quantitative comparison, the results from all investigated models and length scales are displayed in Fig. 4 in terms of the absolute deviation from the isotropic region as described in Section IV.B. As intended, the deviation for isotropic cells, i.e., aspect ratio of 1, is zero for all models. For aspect ratios of 2 the deviation is still very minor for all models except $\Delta_{\max}$. Another commonality between all models is that the deviation is always larger for pencil cells than for pancake cells of the same aspect ratio. Additionally, for high aspect ratio pancake cells all models except for Δ_{vol} show a converging trend of the deviation, i.e., approximately constant or slightly decreasing deviation for higher aspect ratio cells. For pencil cells the error continues to increase for high aspect ratio cells for all models.

The Δ_{vol} length scale is clearly affected the most by anisotropic grids. Especially for high aspect ratio pancake cells the difference to the other investigated models and definitions is extreme.

The two models without an explicit length scale definition, the dynamic Smagorinsky model with 3D filtering and the Vreman model, behave very similarly. For pencil cells the deviation with these models is very close to each other and only slightly less than that for the WALE model with Δ_{vol}. For pancake cells the deviation is again similar, but both models behave much more robustly than the WALE model with Δ_{vol}. For pencil cells the dynamic Smagorinsky model shows slightly larger errors than the Vreman model, but for pancake cells the Vreman model shows slightly worse behavior.

As mentioned above, for aspect ratios of 2, $\Delta_{\max}$ yields the largest deviation out of all models for both pencil and pancake cells. However, a further increase in aspect ratio has relatively little effect on this length scale definition for both cell types. This is especially interesting for high aspect ratio pencil cells for which all other models still show a

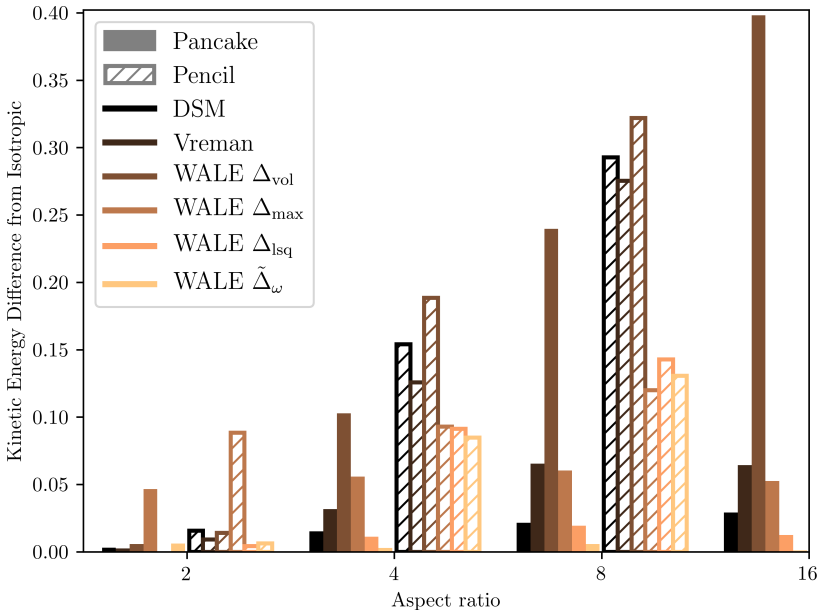

Fig. 4 Deviation from isotropic for all investigated models

strong increase of deviation, leading to Δ_{max} yielding the lowest deviation out of all models for pencil cells with aspect ratio 8. For pancake cells the deviation even decreases slightly again for aspect ratios larger than 8.

The smallest deviations for pancake cells over all aspect ratios are visible for $\widetilde{\Delta}_{\omega}$ and Δ_{lsq}. For both definitions the absolute deviation from the isotropic region is only minimal, with $\widetilde{\Delta}_{\omega}$ slightly superior to Δ_{lsq}. For pancake cells these definitions clearly deliver the best results and while the deviation is larger for pencil cells both definitions are still among the best tested.

For pancake cells Δ_{max}, $\widetilde{\Delta}_{\omega}$ and Δ_{lsq} show a maximum deviation for an aspect ratio of 8 and a slight decrease for higher aspect ratios. This improvement for extreme aspect ratio pancake cells is not caused by an increase in eddy viscosity, but instead the eddy viscosity is indeed slightly lower for higher aspect ratios as would be expected upon refinement. However, the reduction in eddy viscosity is minimal and is more than made up for by the additional resolved turbulence at some point. To check the behavior for even higher aspect ratios, $\widetilde{\Delta}_{\omega}$ was tested for cells with an aspect ratio of 32 as well and the resulting spectrum was located in between those for aspect ratios 8 and 16, thus confirming a converging behavior. This also seems plausible since the length scale for those three definitions does not seem to change significantly for aspect ratios larger than 10 for the *a priori* assessment. This characteristic of the length scales to converge to a certain limit seems to lead to a significantly increased robustness to high aspect ratio cells. A similar behavior can be observed for the pencil cells. While the deviation for $\widetilde{\Delta}_{\omega}$ and Δ_{lsq} increases drastically for aspect ratios of 4, the further increase at aspect ratios of 8 is much lower, indicating a form of convergence for these length scales - just at higher aspect ratios. This would again fit with observations from the *a priori* assessment that show a constant length scale for $\widetilde{\Delta}_{\omega}$ and Δ_{lsq} for aspect ratios larger than about 30.

V. Wall-modeled channel flow

We next assess the effects of grid anisotropy in a more physically meaningful flow than isotropic turbulence. The flow of choice here is the turbulent channel flow at $Re_\tau \approx 5200$ ($Re_b = 125,000$), which is a sufficiently high Reynolds number to require the modeling of the energetic turbulence near the wall. We focus on the predicted mean velocity gradient in the log-layer, a quantity which is independent of the wall-model (for the specific wall-modeling approach used here) and unaffected by viscous processes at this Reynolds number; as a result, the test case should be representative of shear layers more broadly. This is the main reason for choosing this high-Re flow rather than a more standard low-Re channel, which primarily tests the ability of the LES to resolve the viscous buffer layer.

A. Problem set-up

The computational domain is taken as 12.8 δ long and 4.8 δ wide, where δ is the channel half-width. The base grid is chosen to have 192×60×72 grid points, for a wall-parallel grid-spacing of $\Delta x/\delta = \Delta z/\delta = 0.0667$. The wall-normal grid-spacing is gently stretched from $\Delta y_w/\delta = 0.0222$ at the wall to $\Delta y_c/\delta = 0.0444$ at the centerline. At the upper edge of the region of interest ($y/\delta = 0.2$), $\Delta y/\delta = 0.0265$.

An equilibrium wall-model [19, 20] (effectively an instantaneous application of the log-law) is used to compute the instantaneous wall stress τ_w from the instantaneous velocity at a height $h_{\text{wm}}/\delta = 0.1$ above the wall. Note that the LES grid is defined all the way down to the wall, and that the grid-spacing in the LES grid is decoupled from the "interface location" at $y = h_{\text{wm}} = 0.1\delta$. This decoupled approach implies that the LES solution below $y = h_{\text{wm}}$ does not affect the predicted wall shear stress and also allows for the LES grid to be refined without affecting the action of the wall-model; together, these attributes allow for a complete elimination of the so-called "log-layer mismatch" which is the most significant error in wall-modeled LES. The approach is described most clearly in Larsson et al. [20].

We then consider 7 differently refined grids, all of which are refined by a factor of 4 in each direction: grids refined in the x-, y- or z-directions; grids refined in the xy-, xz- or yz-planes; and a grid that is refined in all three directions. The choice of refining by a factor of 4 is done to impart a significant change in grid-spacing without having to compute as many cases as for the forced isotropic turbulence problem. While the computational cost of running these wall-modeled channels is not prohibitive for a single case, the total cost after considering multiple models is quite significant: the results shown here required several million core-hours.

The bulk Mach number is 0.5, which is sufficiently low to avoid any significant variable-property effects without incurring a too severe acoustic time-step limitation. The simulations are run for a time of at least 100 δ/U_b to remove the initial transients, and then averages are collected for a time of about 400 δ/U_b. This has been found to be sufficient in prior studies using similar domain sizes [21].

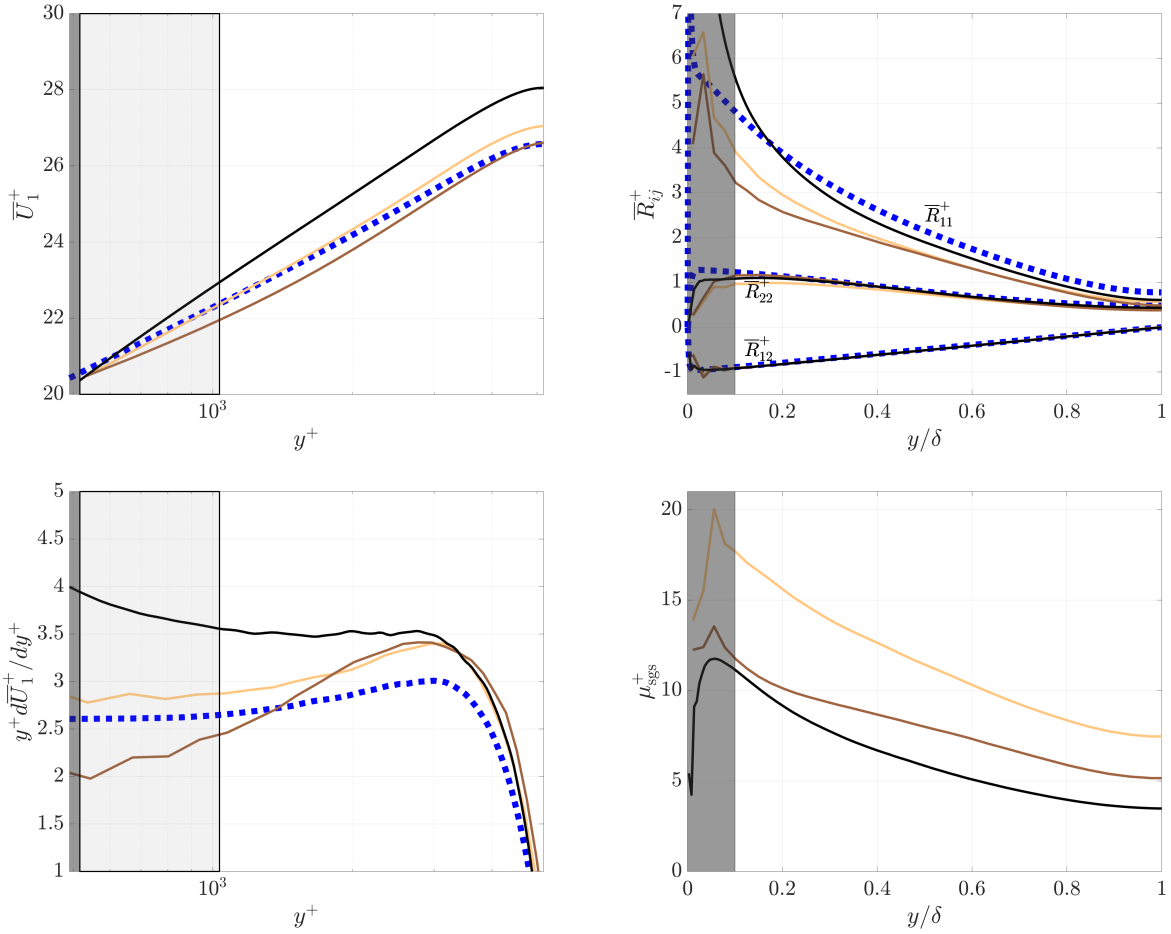

Fig. 5 Representative sample results for the channel flow using the WALE model with the $\widetilde{\Delta}_\omega$ length scale on the base grid with 192×60×72 points (yellow line), z-refined 192×60×288 (brown; lowest velocity gradient), and xy-refined 768×240×72 (black; highest velocity gradient). Compared to the DNS by Lee and Moser [22] (thick dotted line). The dark gray region marks where the wall-model is applied and where the LES result should be discounted. The light gray region shows where κ_{scaled} is defined based on the mean velocity gradient.

B. Sample results and error definition

Representative sample results are shown in Fig. 5. Other models and length scales produce similar results, with an overpredicted mean velocity gradient in the log-layer for the xy-refined grid and an underpredicted mean velocity gradient for the z-refined grid. The figure also shows the mean eddy viscosity, which is decreased (as expected) on the refined grids.

The main quantity-of-interest is chosen to be the slope of the mean velocity profile in the region $h_{\text{wm}} \leq y \leq 2h_{\text{wm}}$, i.e., the slope of the mean velocity profile in the approximate log-layer above the wall-modeled region. Specifically, we compute the implied or effective value of the von Karman coefficient as

$$\kappa_{\text{num}} = \frac{\ln\left(2h_{\text{wm}}^+\right) - \ln\left(h_{\text{wm}}^+\right)}{U_{\text{VD}}^+\left(2h_{\text{wm}}^+\right) - U_{\text{VD}}^+\left(h_{\text{wm}}^+\right)}, \tag{1}$$

where U_{VD} is the Van Driest transformed mean velocity profile. Note that κ_{num} can equivalently be written as the average of $y^+ dU^+/dy^+$ in a logarithmically scaled coordinate, i.e., as the average of the $y^+ dU^+/dy^+$ curves in Fig. 5. The use of a variable-property velocity transformation is arguably not needed at this low Mach number, but is used anyway; also note that the errors in the Van Driest transformation for cold walls (the channel is weakly cooled) are confined to the viscous region and thus will not affect κ_{num}. To get a quantity of order unity, we then consider the scaled value $\kappa_{\mathrm{scaled}} = \kappa_{\mathrm{num}}/\kappa_{\mathrm{ref}}$, where $\kappa_{\mathrm{ref}} = 0.384$ from the DNS of Lee and Moser [22]. When interpreting the sensitivity of κ_{scaled} to changes in the grid, note that small changes $\Delta\kappa_{\mathrm{scaled}}$ are related to changes in the friction coefficient $C_f = 2\tau_w/(\rho U_b^2)$ as* $\Delta C_f/C_f \approx 0.13(\kappa_{\mathrm{scaled}} - 1)$ if we assume that the LES solution is affected by the grid primarily in the region $y \lesssim 2h_{\mathrm{wm}}$. This is plausible since the length scale of the energetic eddies is approximately proportional to the wall distance in the log-layer, which means that the relative grid-spacing (or filter-width) decreases by half over the region of interest and the LES becomes relatively speaking better resolved farther from the wall.

For reference, the three cases in Fig. 5 have κ_{scaled} of 1.17 (z-refined grid, lowest dU^+/dy^+), 0.92 (base grid), and 0.70 (xy-refined grid, highest dU^+/dy^+). These slopes then imply differences in the friction coefficient C_f of about 0.02, -0.01, and -0.04, respectively.

Note that the focus on the mean velocity gradient slope outside in the specific region and the wall-modeling approach (specifically the decoupling of h_{wm} from the LES grid) implies that errors in the wall-model itself do not affect the present analysis: errors in the wall-model would manifest as offsets in the mean velocity profile at $y = h_{\mathrm{wm}}$, which do not enter κ_{scaled}. We specifically avoid the core of the channel partly because this region is relatively better resolved but also in order to minimize the effects of the domain size and averaging time, both of which are expected to have a larger effect on the larger scales of motion in the core of the channel. By focusing on κ_{scaled} we also hope to avoid error cancellations, e.g., cancellations between underpredicted dU/dy in the log-layer and overpredicted dU/dy outside of that which could together produce an exactly predicted skin friction coefficient.

C. Constant coefficient WALE models

The results for the constant coefficient WALE models are listed in Table 1 and plotted (for 6 of the 8 different grids) in Fig. 6. The most striking aspect of the plot is the qualitative similarity between the different length scales. Going counter-clockwise in the plot, all length scales produce a reduced κ_{scaled} for the x-, xy-, and y-refined grids, and then produce an increased κ_{scaled} for the yz-, z-, and xz-refined grids. The xy-refined grid produces the smallest value (i.e., largest velocity gradient) for every length scale, with κ_{scaled} values corresponding to a reduction of the skin friction by between 2.8% and 5.1% on the xy-refined grid for all length scales. The largest κ_{scaled} (smallest velocity gradient) is produced on either the z- or the yz-refined grids, with the two being very close for all length scales.

*To relate the sensitivity of κ_{scaled} to the friction coefficient C_f, we assume that the log-layer mismatch ΔU^+ is constant for $y \gtrsim 2h_{\mathrm{wm}}$ and varies linearly below that point down to $y = h_{\mathrm{wm}}$. The definition of the effective von Karman coefficient (Eqn. 1) then implies (together with a Taylor expansion) that $\Delta U^+ \approx -\ln(2)(\kappa_{\mathrm{scaled}} - 1)/\kappa_{\mathrm{ref}}$, which with $\Delta C_f/C_f \approx -2\Delta U_b^+/U_b^+$ produces $\Delta C_f/C_f \approx 1.7\ln(2)/(\kappa_{\mathrm{ref}}\, U_b^+)(\kappa_{\mathrm{scaled}} - 1) \approx 0.13(\kappa_{\mathrm{scaled}} - 1)$ for the present Reynolds number.

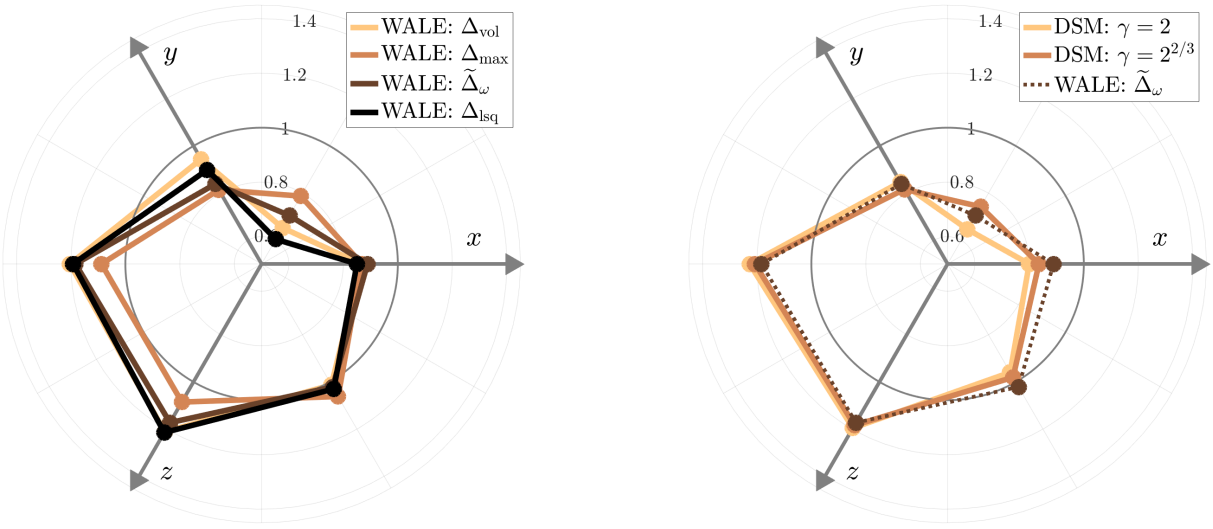

Fig. 6 Scaled von Karman coefficient κ_{scaled} for the channel with different models and length scales. Points along the positive horizontal axis correspond to the x-refined grid; going counter-clockwise, then follows xy-refined, y-refined, yz-refined, z-refined, and the xz-refined grid. The radius of each data point equals $\kappa_{\text{scaled}} - 0.5$.

The Δ_{max} length scale is the most robust to the grid anisotropy, with the least variation between the different grids. However, it is the most sensitive to the grid-spacing itself, with the largest difference between the base and uniformly refined grids (Table 1). The Δ_{vol} and Δ_{lsq} length scales display the largest sensitivities to the grid anisotropy, with $\widetilde{\Delta}_{\omega}$ being marginally better. We note that these channel grids have aspect ratios of at most about 11, which avoids severe pathological behavior from the Δ_{vol} length scale: if grids with much higher aspect ratios were considered, those results would presumably be significantly worse. Interestingly, the length scales with the largest sensitivity to the grid anisotropy show the smallest sensitivity to the isotropic grid refinement, and vice versa.

A very important distinction between the two different test cases used in this study is that the optimal aspect ratio of the grid is known *a priori* for isotropic turbulence (the isotropic grid is obviously optimal) whereas it is not known for the channel case. In addition, the optimal grid aspect ratio should vary across the channel. For these reasons, neither the

Model	base	x-ref	y-ref	z-ref	xy-ref	xz-ref	yz-ref	xyz-ref
WALE: Δ_{vol}	0.935	0.866	0.944	1.211	0.653	1.012	1.203	0.958
WALE: Δ_{max}	0.882	0.868	0.814	1.085	0.787	1.062	1.088	1.018
WALE: $\widetilde{\Delta}_{\omega}$	0.918	0.889	0.839	1.173	0.705	1.021	1.183	0.967
WALE: Δ_{lsq}	0.952	0.850	0.899	1.214	0.605	1.030	1.192	0.929
DSM: $\widehat{\Delta}/\Delta = 2^{2/3}$	0.899	0.835	0.816	1.184	0.742	0.980	1.207	0.999
DSM: $\widehat{\Delta}/\Delta = 2$	0.955	0.799	0.847	1.196	0.646	0.959	1.226	0.958

Table 1 Scaled von Karman coefficient κ_{scaled} for the channel cases with different models/length scales and differently refined grids.

base grid nor the uniformly refined grid can be viewed as the "correct" one that gives the "correct" results, with any deviations then defined as erroneous. We therefore instead look at how the mean velocity gradient changes when the grid changes, i.e., how κ_{scaled} changes when moving from one grid to another. This is done here using simple analysis inspired by design-of-experiments (DOE) thinking. We start by defining the variables X, Y, and Z as being -1 or 1 for grids in which the grid-spacing in the corresponding direction is either at its base level or refined level. For example, the base grid has (X, Y, Z) of $(-1, -1, -1)$ while the xz-refined grid has $(1, -1, 1)$. An additive model for κ_{scaled} is then

$$\kappa_{\text{scaled}} = \alpha_0 + \alpha_x X + \alpha_y Y + \alpha_z Z, \tag{2}$$

which can be solved for the α_* coefficients using least squares for each model/length-scale combination. The accuracy of this linear additive model is assessed in Fig. 7. The good agreement with the actual results shows that so-called "interaction effects" (using the language of design-of-experiments) are small in this problem, i.e., that the effect of grid-refinement in any one direction is relatively insensitive to the grid-spacing in the other two directions (for the rather narrow range of grid-spacings considered here). This implies that we can (or even should) look at the effects of grid-refinement in one direction at a time, and independently of the initial grid. For example, we can quantify the effect of x-refinement by taking the average of the changes in κ_{scaled} for the following four grid-changes: base $\rightarrow$ x-refined, y-refined $\rightarrow$ xy-refined, z-refined $\rightarrow$ xz-refined, and yz-refined $\rightarrow$ xyz-refined. In fact, the α_x coefficient is half of this average.

Figure 8 shows the results of this analysis for each model. The most striking observation is how z-refinement produces a significant positive change in κ_{scaled} (i.e., an increase in the friction coefficient) for all models and all starting grids (the range is always above 0). Similarly, but less pronounced, x- and y-refinement produce negative changes in κ_{scaled} for essentially all models and starting grids.

The second most striking observation is how small the difference is between the different models and length scales, with the exception of $\Delta_{\max}$. Given the large differences in the length scales for the isotropic turbulence problem, it would be reasonable to expect similar differences here; however, they are largely absent. This is a rather negative statement about the current state-of-the-art in LES: the results are strongly affected by the aspect ratio of the grid, even for starting grids that differ in resolution by factors of 4, and even with elaborate definitions of the length scale.

The $\Delta_{\max}$ length scale clearly has the lowest variation between the different starting grids, but still displays the same large effect of z-refinement as the other length scales.

D. Dynamic Smagorinsky model

When used with the Smagorinsky model, the dynamic procedure [11, 12] computes the product $C_{\text{D}}\Delta^2$ of the model coefficient and the length scale for a user-specified test-filter and assumed ratio of the length scales at the test-filtered

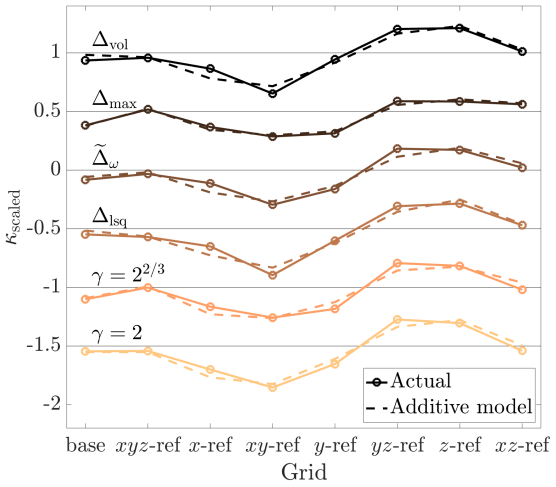

Fig. 7 Effective scaled von Karman coefficient κ_{scaled} for the channel test case (solid lines) compared to the additive model (Eqn. 2; dashed). The results for each model are offset vertically.

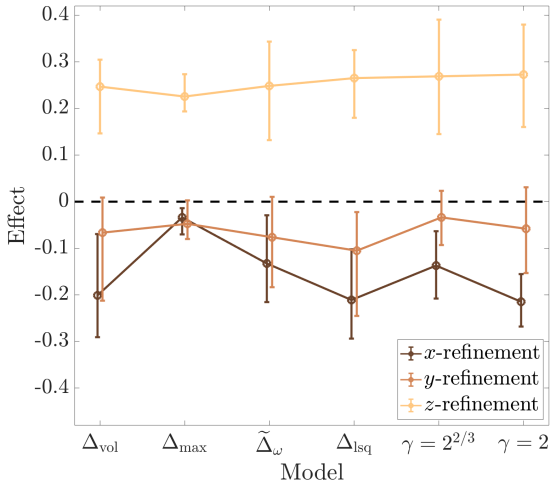

Fig. 8 The effects of unidirectional grid-refinement on the κ_{scaled} for the channel test case. Given for each model, with the circle showing the mean effect while the error bar shows the range of the 4 different refinement steps.

and base levels, i.e., $\gamma = \widehat{\Delta}/\Delta$. For 3D isotropic test-filtering, where the test-filter coarsens by an equal factor in every direction, the definition of the length scale Δ drops out and is irrelevant. However, for any other test-filter, the definition of the length scale becomes important in setting the filter ratio γ.

The traditional approach in channel flows has been to perform filtering (and averaging, although that does not enter into this discussion) in wall-parallel planes. This is typically motivated by a combination of: (i) the assumption that the wall-normal (y) direction is over-resolved; and (ii) the fact that wall-parallel filtering produces no commutation error. Assuming a filter-width ratio of 2 in a single dimension, this will produce filter-width ratios for wall-parallel filtering of $\gamma_{\text{vol}} = \widehat{\Delta}_{\text{vol}}/\Delta_{\text{vol}} = 2^{2/3} \approx 1.6$ and $\gamma_{\text{max}} = \widehat{\Delta}_{\text{max}}/\Delta_{\text{max}} = 2$ for those two length scales. Therefore, use of the dynamic procedure does not remove the need for choosing a length scale definition when performing anything other than isotropic 3D test-filtering.

In the present study we compare results using the DSM model with planar filtering and averaging and two different values of the filter-width ratio γ, specifically the values 2 and $2^{2/3} \approx 1.6$. The first is chosen since it is presumably very common in many LES codes (e.g., it is the default in the *Hybrid* code) while the second is chosen as a reasonable perturbation of the base value: while the second value technically comes from assuming a Δ_{vol} length scale, we are using it here as a possible different value of γ rather than any endorsement of the Δ_{vol} length scale. Note that we want a geometry-only definition of the length scale when choosing the value of γ.

The resulting κ_{scaled} values are included in the same figures and tables as discussed above for the WALE models. While the results with the different γ ratios are qualitatively similar, it is clear that $\gamma = 2^{2/3} \approx 1.6$ leads to lower

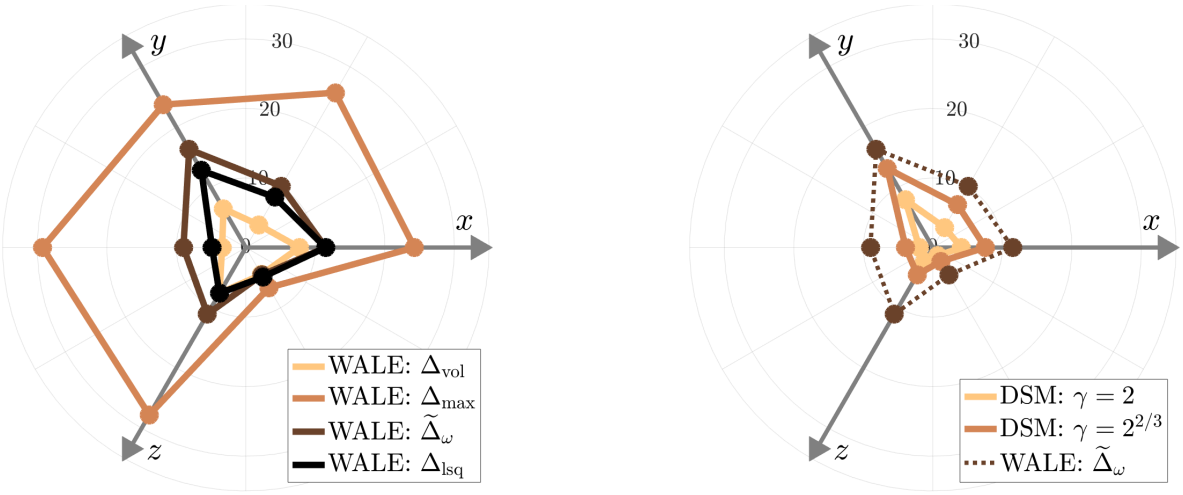

Fig. 9 Mean eddy viscosity μ^+_{sgs} for the channel with different models and length scales. The interpretation of the polar plot is explained in Fig. 6.

sensitivity to the grid anisotropy, particularly for x- and y-refinement. This qualitatively agrees with the findings for the isotropic turbulence problem which showed large errors for 1D filtering with $\gamma = 2$ but an improved behavior with lower γ.

When comparing the results for the dynamic Smagorinsky model to those obtained with the constant coefficient WALE model, it can be observed that both models behave very similarly. This is especially true for WALE with $\widetilde{\Delta}_{\omega}$ and DSM with $\gamma = 2^{2/3}$, for which the relative changes between grids differ only marginally. This is particularly interesting since the mean μ^+_{sgs} values (shown in Fig. 9) are always lower for the DSM model, sometimes by more than a factor of 2.

E. Eddy viscosity and length scale behavior

The mean subgrid eddy viscosity μ_{sgs} is plotted (for 6 of the 8 different grids) in Fig. 9. The scalar values for each case are obtained by averaging over the region $h_{wm} \leq y \leq 2h_{wm}$ where the error is defined.

Comparing these mean μ_{sgs} results with the corresponding κ_{scaled} values in Table 1 and Fig. 6, it is interesting to note that the Δ_{vol} and Δ_{max} length scales produce very similar results on the x-refined grid and yet have mean μ_{sgs} values that differ by a factor of 3. Analogously, the $\widetilde{\Delta}_{\omega}$ and Δ_{lsq} length scales produce similar mean μ_{sgs} values but different κ_{scaled} on this grid. In general, a larger eddy viscosity should lead to both a larger modeled stress and a reduced resolved stress; the exact balance thereof determines how the error behaves. The results highlighted here suggest that this process cannot be understood simply from the mean eddy viscosity, and hence that variations in it, either fluctuations around the mean and/or the wall-normal distribution, must also be important.

It is interesting to note that the WALE models produce much larger variations in μ_{sgs} than the DSM models, with coefficients-of-variation (CV; the standard deviation divided by the mean) that are about 2.5-3 times larger on all grids

and with all length scales. This much larger variation in μ_{sgs} is therefore due to the velocity scale in the WALE model, not the length scale. Having said that, the Δ_{lsq} length scale does produce about 20% larger CV than the other length scales for every grid. Whether a large variation in μ_{sgs} is desirable or not from an accuracy point-of-view is not known; however, extreme values of μ_{sgs} can lead to time step restrictions in codes with explicit time stepping. In the present study, the time step was generally limited by the convective spectral radius on 5 out of 8 grids (which resulted in the same time step for all models except Δ_{max}) but by the diffusive spectral radius for the y-, xy-, and yz-refined grids. On those grids, the WALE model with the Δ_{vol} length scale produced approximately the same time steps as the DSM models, but time steps that were lower by factors between 3.4-4.5 for Δ_{max}, 3.3-4.4 for Δ_{lsq}, and 1.2-2.4 for $\widetilde{\Delta}_{\omega}$. Therefore, while the WALE velocity scale produces large variations in μ_{sgs}, the impact on the time step required some intricate coupling with the length scale in the present study. The potential for severely reduced time steps for particularly the Δ_{max} and Δ_{lsq} length scales and to a lesser extent $\widetilde{\Delta}_{\omega}$ is not an insignificant drawback.

To see the spatial variation across the channel, contours of the empirical probability density functions (pdfs) of the length scale are shown in Fig 10 for some representative cases. The $\widetilde{\Delta}_{\omega}$ length scale produces a very narrow distribution in this flow across the full channel, which again illustrates clearly that the large variations in μ_{sgs} with WALE are due entirely to the velocity scale. We note that the $\widetilde{\Delta}_{\omega}$ length scale is bounded from above by the Δ_{L2} length scale; for this flow and grid, the mean $\widetilde{\Delta}_{\omega}$ is close to this upper bound throughout the channel. The Δ_{lsq} length scale produces much larger variations, almost reaching the geometric extremes of the cell size with finite probability throughout the whole channel. This length scale also produces qualitatively different results on different grids. The most likely value of Δ_{lsq} tends to the wall-normal Δy very close to the wall on all grids. This is most likely due to the underresolved solution very near the wall (in fact, in the wall-modeled layer, where the LES solution is not to be trusted; cf.[20]) becoming mainly dominated by wall-normal gradients with unrealistic turbulence. Away from the wall, the most likely value tends to Δy on the x- and z-refined grids but to $\min\{\Delta x, \Delta z\}$ on all other grids.

VI. Effect of the model coefficient

For the fixed constant models, the sensitivity of the subgrid model to anisotropy-induced errors in the computed filter length also depends on the chosen model coefficient. This is because the model coefficient determines whether the subgrid model computes too much or too little eddy viscosity, which influences how the model reacts to inaccuracies in the filter length computation. Intuitively one might expect a larger model coefficient to produce results that are less sensitive to the grid anisotropy due to the reduced small-scale resolved motions. An alternative line of thought is that a larger model coefficient amplifies changes in the length scale between different grids and thus produces a larger sensitivity to the grid anisotropy. The hypotheses differ partly due to whether one focuses on the effect of grid anisotropy on the numerical error (hypothesis I: larger coefficient leads to smaller sensitivity) or the modeling error (hypothesis II: larger coefficient leads to larger sensitivity).

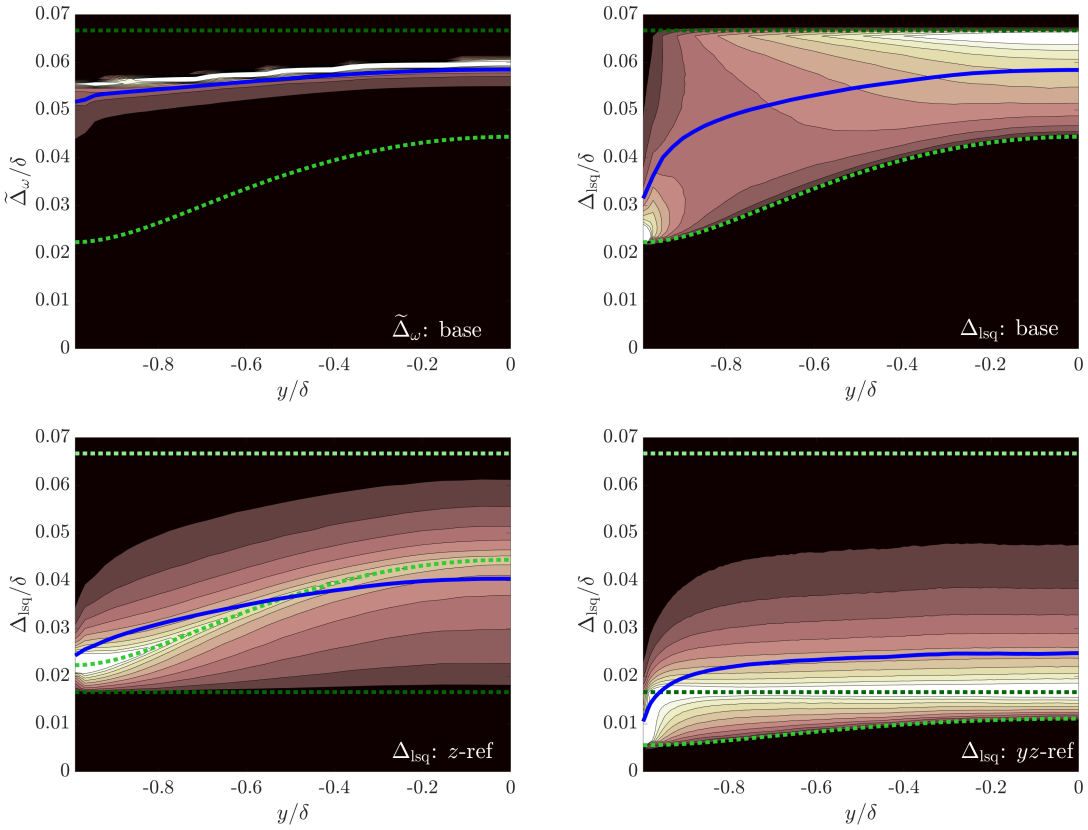

Fig. 10 Empirical probability density functions of Δ for the channel flow with the WALE model, comparing $\widetilde{\Delta}_\omega$ (top left; showing the base grid which is representative of all grids) with Δ_{lsq} on the base grid (top right, also representative of the y- and xz-refined), z-refined grid (bottom left, also representative of the x-refined), and the yz-refined grid (bottom right, also representative of the xy-refined). The solid line is the mean length scale, while the dotted lines show the Δx, Δy and Δz grid-spacings.

The hypothetical cases of setting the model coefficient to very large or very small values favors hypothesis II. If the model coefficient is set to zero, the eddy viscosity is always zero and thus inaccuracies in the length scale definition have no effect; if the model coefficient is set as large as possible without laminarizing the flow, even small differences in the length scale would produce large changes in the eddy viscosity which would then presumably have a large effect on this very (effectively) low-*Re* turbulence. In other words, a larger model coefficient should then produce the largest sensitivity to the grid anisotropy.

For reasonable values of the model coefficient, an increased coefficient would instantaneously produce larger eddy viscosity which would then reduce the small-scale content of the velocity field, which would then relax the eddy viscosity downwards. While the nonlinearity of this process prevents any hard statements, common LES experience is that a larger model coefficient produces a larger μ_{sgs} for a given grid; this then directly implies that a larger model coefficient produces an eddy viscosity in which the square of the length scale is multiplied by a larger factor (the coefficient times the velocity scale). Hence this reasoning also supports hypothesis II, that a larger model coefficient should lead to larger

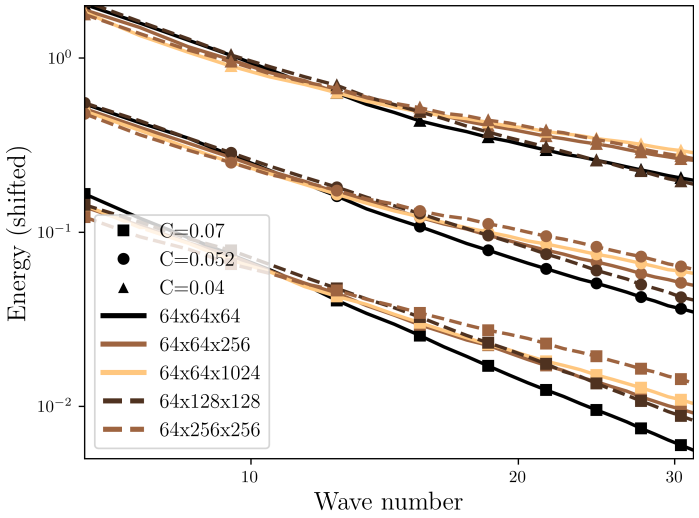

Fig. 11 Comparison of spectra for the Vreman model with different model constants. The spectra for the two smaller model constants are shifted upwards for better clarity.

sensitivity to the grid anisotropy.

This type of behavior is in fact observed in the forced isotropic turbulence test case. Figure 11 shows spectra from the Vreman model with three different model coefficients: $C_V = 0.07$, $C_V = 0.052$ and $C_V = 0.04$. The sensitivity to the grid anisotropy is related to the spread between the spectra on different grids for each respective model constant. The smallest model coefficient $C_V = 0.04$ produces the smallest spread between the different grids while the largest model coefficient $C_V = 0.07$ produces the largest spread.

The channel test case produces less clear results on this issue. Some results are listed in Table 2. A higher model coefficient always leads to smaller κ_{scaled}, i.e., a reduced friction coefficient. The sensitivity to grid anisotropy is manifested in the change in κ_{scaled} between grids. For z-refinement, all cases in the table (different length scales, different model coefficients) produce approximately the same change of +0.23 to +0.27 in κ_{scaled}, thus neither confirming nor rejecting either of the two basic hypotheses. The effect of x-refinement is -0.03 and -0.10 for the low model coefficient and +0.03 and 0 for the high coefficient, which is actually consistent with hypothesis I (larger coefficient leads to reduced sensitivity) and inconsistent with the forced isotropic turbulence results. The most likely reason is that the channel flow is affected by a larger range of flow physics which may produce competing behaviors.

Model	base	x-ref	z-ref
WALE: $\widetilde{\Delta}_\omega$	0.918 (0.823)	0.889 (0.856)	1.173 (1.056)
WALE: Δ_{lsq}	0.952 (0.849)	0.850 (0.844)	1.214 (1.119)

Table 2 Scaled von Karman coefficient κ_{scaled} for the channel cases with different model coefficients for selected cases. Comparing the standard coefficient $C_W = 0.4$ with the higher value $C_W = 0.8$ (in parentheses).

VII. Summary and discussion

The original objective of this study was to find the "best" subgrid model length scale: ideally a length scale that produces results that are simultaneously accurate and robust with respect to the grid anisotropy, but more realistically some type of compromise between accuracy and robustness. While some of the length scales considered here come close to satisfying that goal for the forced isotropic turbulence problem, none of them produce LES results that are independent of the grid anisotropy for the channel test case.

Our general observations from this study are collected below. We must note, however, that these observations are strictly true only for the particular code and grids used here; it is entirely possible that a code with different numerics would produce different results. The present results should be viewed as a "snapshot" or a single realization, indicative of LES methods but not necessarily universally true.

A. Observations on the constant coefficient model results

As expected, the $\Delta_{\max}$ length scale is the most robust to the grid anisotropy when taking into account both problems considered here, while the commonly used Δ_{vol} length scale is the least robust, with the inconsistent behavior of going to zero for repeated anisotropic refinement. The more advanced, flow-dependent, length scales $\widetilde{\Delta}_\omega$ and Δ_{lsq} were found to be very robust for the isotropic turbulence problem but were found much less robust for the channel problem which is a more complex flow. $\widetilde{\Delta}_\omega$ seemed slightly superior to Δ_{lsq} in the isotropic turbulence problem for the code used here and - while similar in terms of sensitivity - did show less extreme time step limitations than Δ_{lsq}. The Vreman model, which has a built-in length scale, is relatively robust to pancake cells but less so to pencil cells. It shows larger sensitivity to the grid anisotropy than the WALE model with either $\widetilde{\Delta}_\omega$ or Δ_{lsq}.

A somewhat surprising result (at least to the authors) is the fact that simply increasing the model coefficient does not reduce the sensitivity to the grid anisotropy, and actually makes it worse in the forced isotropic turbulence problem considered here. The interpretation is that the reduced numerical error of a larger model coefficient is more than compensated by an increased modeling error, and since this modeling error is affected by grid anisotropy through the length scale the overall sensitivity may go up.

We also note that the WALE model produced 2-3 times larger fluctuations in the eddy viscosity in this study, which resulted in reduced time steps for some grids and length scales (up to 2.4 times smaller for $\widetilde{\Delta}_\omega$, up to 4.4 times smaller for Δ_{lsq}). The propensity of subgrid models to produce extremely large μ_{sgs} values should be taken into account when developing or assessing subgrid models. Spatial low-pass filtering of the eddy viscosity may reduce this problem, but would redistribute the eddy viscosity and thus create an additional parameter that would have to be tuned.

B. Observations on the dynamic Smagorinsky results

When used with full 3D isotropic test-filtering, the dynamic Smagorinsky model with filter-ratio $\gamma = 2$ was found to be robust to pancake cells but less robust to pencil cells, with energy pile-up at the highest wavenumbers for the isotropic turbulence problem.

A curious result of this study is the behavior of the dynamic Smagorinsky model when applied with less than 3D test-filtering, i.e., when test-filtering in only one or two directions: the method produces better results for both the isotropic turbulence case and the channel case when the filter width ratio $\gamma = \widehat{\Delta}/\Delta$ is computed based on the Δ_{vol} length scale (i.e., $\gamma = 2^{1/3}$ for the 1D test-filtering in the isotropic turbulence problem, and $\gamma = 2^{2/3}$ for the 2D test-filtering in wall-parallel planes in the channel) rather than the Δ_{max} length scale ($\gamma = 2$ for both problems). This is curious since the Δ_{vol} length scale is objectively inconsistent in terms of its limiting behavior when subjected to repeated anisotropic refinement. Therefore, the dynamic Smagorinsky model produces (in this study) the best results with the least plausible length scale. Further investigation into the behavior of DSM with less than 3D filtering on anisotropic grids seems warranted.

As expected, the dynamic procedure fails when test-filtering is applied only to an already refined direction, especially in the case of pancake cells.

C. Implications for LES

The observations above lead to at least two different important implications for the development and use of LES models.

The first is that the LES community may have to re-think the idea of tying the subgrid modeling length scale to the grid, at least in the context of eddy viscosity subgrid models. Note that this also applies to many studies that do "explicitly filtered LES" where the filter width is taken as fixed under grid-refinement, since the filter width is often taken as proportional to the grid-spacing and thus inherits the same anisotropy as (and thus sensitivity to) the grid [23, 24]. There have been attempts to develop subgrid eddy viscosity models without any reference to the grid, e.g., the method of Piomelli et al. [25] where the length scale is estimated from the flow field. In light of the findings of the present study, robustness to grid anisotropy should be viewed as a real strength of such approaches. In a similar vein, it is at least theoretically possible that subgrid models that do not rely on the eddy viscosity hypothesis may be more robust to the grid anisotropy. If that is the case, this would be a motivation to move towards such models.

The second general observation is that this study makes it glaringly obvious that one must never assess LES models on a single grid, or even on a sequence of refined grids that have the same grid anisotropy. It should be absolutely mandatory to assess models on grids with both different refinement levels and different grid anisotropies. Note that every single model and length scale combination in Table 1 produces good agreement with DNS ($\kappa_{\text{scaled}} \approx 1$) on at least one grid – hence all of these models and length scales could have been declared "very good" in a study conducted with

grids of a single aspect ratio. Put another way: 5 of the 6 models in the Table produce the best agreement with DNS on at least one grid, and hence 5 of the 6 models could have been declared the "winner" in a comparative study done on grids with a single aspect ratio.

Funding Sources

This work has been supported by NSF grant CBET-1804825 (ST, JL) and the German Research Foundation (Deutsche Forschungsgemeinschaft – DFG) in the framework of the Sonderforschungsbereich Transregio 40 (JES).

Computing time has been provided by the University of Maryland supercomputing resources and the Argonne Leadership Computing Facility under the INCITE program.

References

[1] Carati, D., and Cabot, W., "Anisotropic eddy viscosity models," *Proc. Summer Program, Center for Turbulence Research*, 1996.

[2] Haering, S. W., Lee, M., and Moser, R. D., "Resolution-induced anisotropy in large-eddy simulations," *Phys. Rev. Fluids*, Vol. 4, 2019, p. 114605.

[3] Stolz, S., and Adams, N. A., "An Approximate Deconvolution Procedure for Large-Eddy Simulation," *Phys. Fluids*, Vol. 11, No. 7, 1999, pp. 1699–1701.

[4] Clark, R. A., Ferziger, J. H., and Reynolds, W. C., "Evaluation of subgrid-scale models using an accurately simulated turbulent flow," *J. Fluid Mech.*, Vol. 91, 1979, pp. 1–16.

[5] Vreman, B., Geurts, B., and Kuerten, H., "Large-eddy simulation of the temporal mixing layer using the Clark model," *Theo. Comput. Fluid Dyn.*, Vol. 8, 1996, pp. 309–324.

[6] Chauvet, N., Deck, S., and Jacquin, L., "Zonal detached eddy simulation of a controlled propulsive jet," *AIAA J.*, Vol. 45, No. 10, 2007, pp. 2458–2473.

[7] Mockett, C., Fuchs, M., Garbaruk, A., Shur, M., Spalart, P., Strelets, M., Thiele, F., and Travin, A., "Two non-zonal approaches to accelerate RANS to LES transition of free shear layers in DES," *Progress in hybrid RANS-LES modelling*, Springer, 2015, pp. 187–201.

[8] Trias, F., Gorobets, A., Silvis, M., Verstappen, R., and Oliva, A., "A new subgrid characteristic length for turbulence simulations on anisotropic grids," *Phys. Fluids*, Vol. 29, No. 11, 2017, p. 115109.

[9] Vreman, A., "An eddy-viscosity subgrid-scale model for turbulent shear flow: Algebraic theory and applications," *Phys. Fluids*, Vol. 16, No. 10, 2004, pp. 3670–3681.

[10] Nicoud, F., and Ducros, F., "Subgrid-scale stress modelling based on the square of the velocity gradient tensor," *Flow, Turb. Comb.*, Vol. 62, No. 3, 1999, pp. 183–200.

[11] Germano, M., Piomelli, U., Moin, P., and Cabot, W. H., "A dynamic subgrid-scale eddy viscosity model," *Phys. Fluids A*, Vol. 3, No. 7, 1991, pp. 1760–1765.

[12] Lilly, D. K., "A Proposed Modification of the Germano Subgrid-Scale Closure Method," *Phys. Fluids*, Vol. 4, No. 3, 1992, pp. 633–635.

[13] Deardorff, J. W., "A numerical study of three-dimensional turbulent channel flow at large Reynolds numbers," *J. Fluid Mech.*, Vol. 41, No. 2, 1970, pp. 453–480.

[14] Spalart, P. R., "Comments on the feasibility of LES for wings, and on a hybrid RANS/LES approach," *Proc. First AFOSR International Conference on DNS/LES*, Greyden Press, 1997.

[15] Ducros, F., Laporte, F., Souleres, T., Guinot, V., Moinat, P., and Caruelle, B., "High-order fluxes for conservative skew-symmetric-like schemes in structured meshes: application to compressible flows," *J. Comput. Phys.*, Vol. 161, 2000, pp. 114–139.

[16] Mattsson, K., Svärd, M., and Nordström, J., "Stable and accurate artificial dissipation," *J. Sci. Comp.*, Vol. 21, 2004, pp. 57–79.

[17] Vasilyev, O. G., Lund, T. S., and Moin, P., "A general class of commutative filters for LES in complex geometries," *J. Comput. Phys.*, Vol. 146, 1998, pp. 82–104.

[18] Trettel, A., and Larsson, J., "Mean velocity scaling for compressible wall turbulence with heat transfer," *Phys. Fluids*, Vol. 28, No. 2, 2016, p. 026102.

[19] Kawai, S., and Larsson, J., "Wall-modeling in large eddy simulation: length scales, grid resolution and accuracy," *Phys. Fluids*, Vol. 24, 2012, p. 015105.

[20] Larsson, J., Kawai, S., Bodart, J., and Bermejo-Moreno, I., "Large eddy simulation with modeled wall-stress: recent progress and future directions," *JSME Mech. Eng. Reviews*, Vol. 3, 2016.

[21] Toosi, S., and Larsson, J., "Anisotropic grid-adaptation in large eddy simulations," *Comput. Fluids*, Vol. 156, 2017, pp. 146–161.

[22] Lee, M., and Moser, R. D., "Direct numerical simulation of turbulent channel flow up to $Re_\tau \approx 5200$," *J. Fluid Mech.*, Vol. 774, 2015, pp. 395–415.

[23] Gullbrand, J., and Chow, F. K., "The Effect of Numerical Errors and Turbulence Models in Large-Eddy Simulations of Channel Flow, With and Without Explicit Filtering," *J. Fluid Mech.*, Vol. 495, 2003, pp. 323–341.

[24] Bose, S. T., Moin, P., and You, D., "Grid-independent large-eddy simulation using explicit filtering," *Phys. Fluids*, Vol. 22, 2010, p. 105103.

[25] Piomelli, U., Rouhi, A., and Geurts, B. J., "A grid-independent length scale for large-eddy simulations," *J. Fluid Mech.*, Vol. 766, 2015, pp. 499–527.